

Research article

# Effect of ZnO particle size on piezoelectric nanogenerators and mechanical energy harvesting

Kebena Gebeyehu Motora<sup>✉</sup>, Chang-Mou Wu<sup>\*✉</sup>, Gokana Mohana Rani<sup>✉</sup>, Wan-Tzu Yen<sup>✉</sup>

Department of Materials Science and Engineering, National Taiwan University of Science and Technology, 10607 Taipei, Taiwan, R.O.C

Received 10 March 2022; accepted in revised form 16 July 2022

**Abstract.** With the increasing demand for green and renewable energy, piezoelectric nanogenerators (PENGs) are in the infant stage for the next generation of wearable energy supplies. In this study, we synthesize an electrospun poly (vinylidene fluoride) zinc oxide (PVDF@ZnO) PENG device with different particle sizes of ZnO by solution electrospinning and study the effect of incorporation of ZnO and its particle size on the piezoelectric properties of the PVDF PENG device. We evaluate the piezoelectric properties of the PENG device under different mechanical conditions of tension, compression, and bending. The incorporation of ZnO nanoparticles remarkably enhances the piezoelectric response of PVDF under all the study conditions. In particular, the device with large-particle ZnO (PVDF@L-ZnO) PENG generates an electrical output current, voltage, and power density of 1308 nA, 5.6 V, and 2160  $\mu\text{W}/\text{m}^2$ , respectively, at a loading resistance of 10 M $\Omega$  under compression; 42 mV, 82 nA, and 28  $\mu\text{W}/\text{m}^2$ , respectively, at a loading resistance of 20 M $\Omega$  under tension; 2.8 V, 323 nA, and 320  $\mu\text{W}/\text{m}^2$ , respectively, at a loading resistance of 20 M $\Omega$  under bending, and we choose the compression result for further practical applications. In addition, we use the PENG device to harvest waste vibration mechanical energy from an air compressor machine with a frequency of 60 Hz. It harvests waste mechanical energy that turns on a liquid crystal display (LCD). The PVDF@L-ZnO PENG device also shows stable cyclic discharging and charging properties, which are crucial for practical applications. Therefore, the fabricated PENG device is a favorable candidate for wasted mechanical energy and converting it to electrical energy. We expect that it can play an important role in the problems related to renewable and green energy utilization.

**Keywords:** nanocomposites, ZnO particle size, smart polymers, waste mechanical energy-harvesting, nanomaterials

## 1. Introduction

The development of renewable energy generation technology is crucial from an economic and environmental perspective [1, 2]. With the advent of global warming and the energy crisis, energy harvesters have significantly considered generating renewable and green energy [3–9]. Harvesting energy from wasted energy sources that include but are not limited to solar, wind, vibration, and heat is an exciting research topic [10–13]. Amongst these renewable energy sources, mechanical energy generated by mechanical deformation, vehicle movement, human

activity, and vibrations is ubiquitous and can be harvested and utilized for green energy generation [14–18]. Therefore, designing and developing materials that can harvest this energy is crucial. Recently, piezoelectric energy harvesters that can harvest electrical energy from vibration or mechanical loading have gained interest as materials for powering electronic devices in various application areas [19–23] because of their simplicity and scalability [24]. Piezoelectric materials can convert mechanical energy to electrical energy, which plays a significant role in self-powering electronic systems [25–28].

\*Corresponding author, e-mail: [cmwu@mail.ntust.edu.tw](mailto:cmwu@mail.ntust.edu.tw)  
© BME-PT

These materials are categorized into inorganic single crystals and ceramic semiconductors under one class and polymers under another class. Even though inorganic piezoelectric materials exhibit a large piezoelectric coefficient, their brittleness and fragility under continuous applied external force are the main drawbacks that limit their practical application. In contrast, piezoelectric polymers, such as poly(vinylidene fluoride-co-trifluoroethylene) [29], PVDF [30], and poly(vinylidene fluoride co hexafluoropropylene) [31] are flexible, durable, easy to process, tough, and lightweight. These properties make them suitable for use in different areas of application, including actuators, flexible detectors, sensors, wearable electronics, and energy harvesting [32, 33].

PVDF is one of the most significant electroactive polymer because of its distinctive ferroelectricity, pyroelectricity, piezoelectricity, properties, and low cost [34–36]. It has five crystalline phases: the  $\alpha$ -phase, which generally exists in the films of commercial PVDF, is non-polar and most stable, whereas the  $\beta$ -phase has the highest dipole density and highest piezo and pyroelectric activities [37, 38]. Thus, it is crucial to converting the other crystal phases of PVDF into the  $\beta$ -phase. Researchers have developed various methods for converting the  $\alpha$  phase of PVDF to the  $\beta$ -phase, such as electrospinning, high voltage polarization, mechanical stretching, and adding nanofillers [39, 40]. Different nanofillers such as carbon nanotubes [41], graphene [42], graphene oxide [43], silver nanoparticles [44], and gold nanoparticles [45] have been incorporated into PVDF, and they exhibited a rise in  $\beta$ -phase enhancement, which is crucial for piezoelectric properties of PVDF. However, these conductive nanofillers suffer from static charge dissipation and can be added only in limited amounts. Therefore, it is extremely important to select non-conductive nanofillers such as ceramics, especially piezoelectric ceramics, which can synergistically improve the piezoelectric constant ( $d_{33}$ ). Various types of ceramic nanofillers have been used to enhance the piezoelectric and dielectric properties of PVDF [46]. From them, BaTiO<sub>3</sub> and lead-containing perovskites, especially lead zirconate titanate, are the most widely investigated [46, 47]. However, these nanofillers are not eco-friendly and can also affect human health; therefore, it is very important to replace them with other nanofillers [48]. Recently, ZnO has received significant attention as a ceramic nanofiller in the field of piezoelectric energy harvesting.

ZnO is one of the most important environment-friendly multifunctional semiconductors used for different applications such as optoelectronics, energy harvesting, gas sensor, and photocatalysis [49–52]. Recently, its' application has been an active research area, and it exhibited excellent performance in electronic, electromechanical, and electrochemical devices, high-performance nanosensors [53], and nanogenerators [54] because of its outstanding optical and electrical properties as well as its ease of formation into different morphological structures [51]. ZnO is a promising candidate for commercial purposes because of its advantages such as low cost, abundance, chemical stability in the air, high biocompatibility, and a simple and wide range of crystal growth technologies. Recently, the exploitation of the piezoelectric properties of ZnO-based nanogenerators has gained significant attention. For instance, piezoelectric nanogenerators developed from PVDF@ZnO nanocomposite revealed an electrical output voltage of 1.12 V using 140 Hz and 116 dB sound [55]. In another study, PVDF@ZnO nanowire was fabricated, and it exhibited an electrical output voltage of 3.2 V [56]. PVDF@ZnO hybrid-based wearable PENG was fabricated, and it exhibited an output current density and voltage of 10 nA/cm<sup>2</sup> and 0.1 V, respectively [57]. All of these findings display the importance of incorporating ZnO into a PVDF polymer, which exhibited enhanced energy harvesting properties of the developed devices compared with pure PVDF. However, there is no study on the effect of the particle size of ZnO on the piezoelectric property of PVDF-based PENG devices.

The effects of the particle size on the piezoelectric and dielectric constant of different materials have been studied. The effect of the lead zirconate titanate (PZT) particle size on the piezoelectric and dielectric constants was investigated [37, 58–61], and the findings showed that the dielectric constant and piezoelectric property depended on the particle size, and the PZT with the largest particle size exhibited the highest piezoelectric and dielectric constants. In contrast, some studies have also shown that the dielectric and piezoelectric properties of nanofillers with smaller particles are better than those of nanofillers with larger particles [62–64]. However, the effect of the particle size on the dielectric constant and piezoelectric property of PZT perovskite (4.9 and 83.5  $\mu$ m) was also evaluated, and the findings showed that the piezoelectric and dielectric constants improved irrespective of

the particle size [65]. This indicates that the effect of the particle size on the piezoelectric and dielectric constants is unknown. Therefore, this is an important parameter that must be investigated and clarified.

In this study, an electrospun PVDF@ZnO-based PENG device composed of large ZnO (L-ZnO) and small ZnO particles (S-ZnO) was prepared by simple solution electrospinning. The effect of the incorporation of ZnO and its particle size on the piezoelectric properties of PVDF under compression, tension, and bending was studied. The application of the developed PENG device for mechanical energy harvesting, and the utilization of the harvested energy for applications such as LCD turn-on, LED energizing, and capacitor charging were also investigated. The piezoelectric response of the developed PENG device under different types of forces that exist in human body motion has also been reported. The practical applicability of the developed PENG device to harvest the mechanical energy wasted during the usual operation of machines was also evaluated.

## 2. Materials and methods

### 2.1. Materials

Dimethylformamide (DMF, 99.8%, Acros, New Jersey USA), poly(vinylidene fluoride) pellets (Kynar 720, Arkema Group, France), anhydrous ethanol (99.9%, Echo Chemical Co. Ltd., Taiwan), thermoplastic polyester elastomer (TPEE, EM400, Taiwan plastic and polymers Co. Ltd., Taipei Taiwan), acetone (95%, Echo Chemical Co. Ltd., Taiwan), small- (20–40 nm) and large- (200–500 nm) particle ZnO (LIWEI Nano Tech Co. Ltd., Taiwan), copper film (0.1 mm thickness), and Kapton tape were purchased from KWO-YI Ltd. (Taipei, Taiwan). All the materials were used as received from the supplier without further purification.

### 2.2. Preparation of PVDF@ZnO nanofiber membranes

ZnO (10 wt%) was added to DMF (6 ml) and ultrasonicated for 20 min. Subsequently, 2.2 g of PVDF pellet was added to it, and the mixture was stirred at 100 °C for 2 h to prepare the PVDF polymer solution. After cooling to 30 °C, 4 ml of acetone were added to the polymer solution for electrospinning. The electrospinning system consisted of an injection spinneret powered by a syringe pump (KDS 101 Series, KD Scientific, USA) that was connected to a Teflon tube attached to a stainless-steel needle

(0.23 mm diameter). An electrostatic controller (SM 4030 24NIR, You Shang Technical Corp., Taiwan) connected to the spinneret and collector was grounded. The nanocomposites were then directly electrospun. Detailed electrospinning conditions can be found in our previous study [66].

### 2.3. Characterizations

The morphologies of the electrospun nanofiber membranes were characterized by transmission electron microscopy (JEOL JEM-2010, Tokyo, Japan) and field-emission scanning electron microscopy (JSM 6500F, JEOL, Tokyo, Japan). Fourier infrared spectroscopy (FTIR, FTIR-4600, JASCO, Tokyo, Japan) was used to quantify the differences in the crystal phases of the synthesized samples. The crystal structures of the synthesized pure PVDF, PVDF@S-ZnO, and PVDF@L-ZnO fiber membranes were studied by X-ray diffraction analysis using a D2 Phaser X-ray diffractometer (Bruker, Karlsruhe, Germany). The tensile properties of the electrospun nanofiber membranes were studied according to ASTM D882 using a universal testing machine (QC-508M2, Comotech, Taichung, Taiwan). A dumbbell specimen with a gauge length of 33 mm and width of 6 mm was synthesized for the tensile test, and a crosshead speed of 50 mm/min was used. A wide-range D<sub>33</sub> meter (YE2730, APC International Ltd., Mackey Ville, PA, USA) was used to analyze the piezoelectric coefficient of the poled electrospun nanofiber membrane. The measured piezoelectric coefficient ( $d_{33}$ ) was used to evaluate the relationship between piezoelectricity and the degree of crystallization. This system was used to directly evaluate the  $d_{33}$  values of the piezoelectric samples. To characterize the piezoelectric response of the prepared material, an SMU (Keithley 2400, Tektronix Inc., Beaverton, OR, USA) and Pico scope were used, and data were collected using a computer.

### 2.4. Study of piezoelectric response under dynamic compression

For the compression test, the prepared PVDF and PVDF@ZnO nanocomposite samples were cut into circular shapes with a diameter of 4 cm. Then, the fiber membrane was sandwiched between copper foils used as electrodes, in which two polypropylene films as substrates were placed at the bottom and top to make a PENG. The developed PENG was then compressed between two stainless-steel cylinders

using a material testing system. To investigate the piezoelectric properties of the PENG devices, a compressive force from 4 to 16 N was applied at a frequency of 0.16 Hz. Subsequently, the piezoelectric responses were evaluated using a source meter unit (SMU, Keithley 2400).

## 2.5. Piezoelectric response under dynamic tension

To evaluate the piezoelectric response under tension, the as-synthesized fiber membrane was cut into a square of  $3 \times 3 \text{ cm}^2$  and was sandwiched between layers of Au-coated nonwoven-TPEE, which was used as an electrode to maintain the flexibility of the samples. The developed PENG device was then stretched using a universal tensile machine.

## 2.6. Piezoelectric response under dynamic bending

To evaluate the piezoelectric response under dynamic bending, the as-synthesized fiber membrane sample was cut into a  $3 \times 3 \text{ cm}^2$  square, and the copper tape was used as an electrode to maintain the flexibility of the sample, while black Bristol paper was utilized as an insulating layer. The PENG device was fixed using double-sided tape between two acrylic boards and bent at an angle of 10 to  $180^\circ$ . The electrical output values generated at certain bending angles were evaluated, and the average value was reported.

# 3. Results and discussion

## 3.1. Characterization of morphology and crystallinity of electrospun fiber membranes

The surface morphologies of the synthesized samples were studied by using field emission scanning electron microscopy (FESEM), and the results were presented in Figure 1. The surface morphology of pure PVDF fiber membrane shows successful preparation fiber membrane with  $165 \pm 50 \text{ nm}$  average diameter as presented in Figure 1a and the morphology of fiber membrane was not significantly affected after incorporation of small ZnO (Figure 1b) and large ZnO (Figure 1c). Furthermore, the existence of ZnO was also evaluated using TEM and the result is displayed in Figure 1d shows that ZnO nanoparticles of average particle 20–40 nm aggregated on the PVDF fiber membrane for PVDF@S-ZnO were observed. While in the case of PVDF@L-ZnO, nanoparticles of average particle size 200–400 nm are aggregated on the

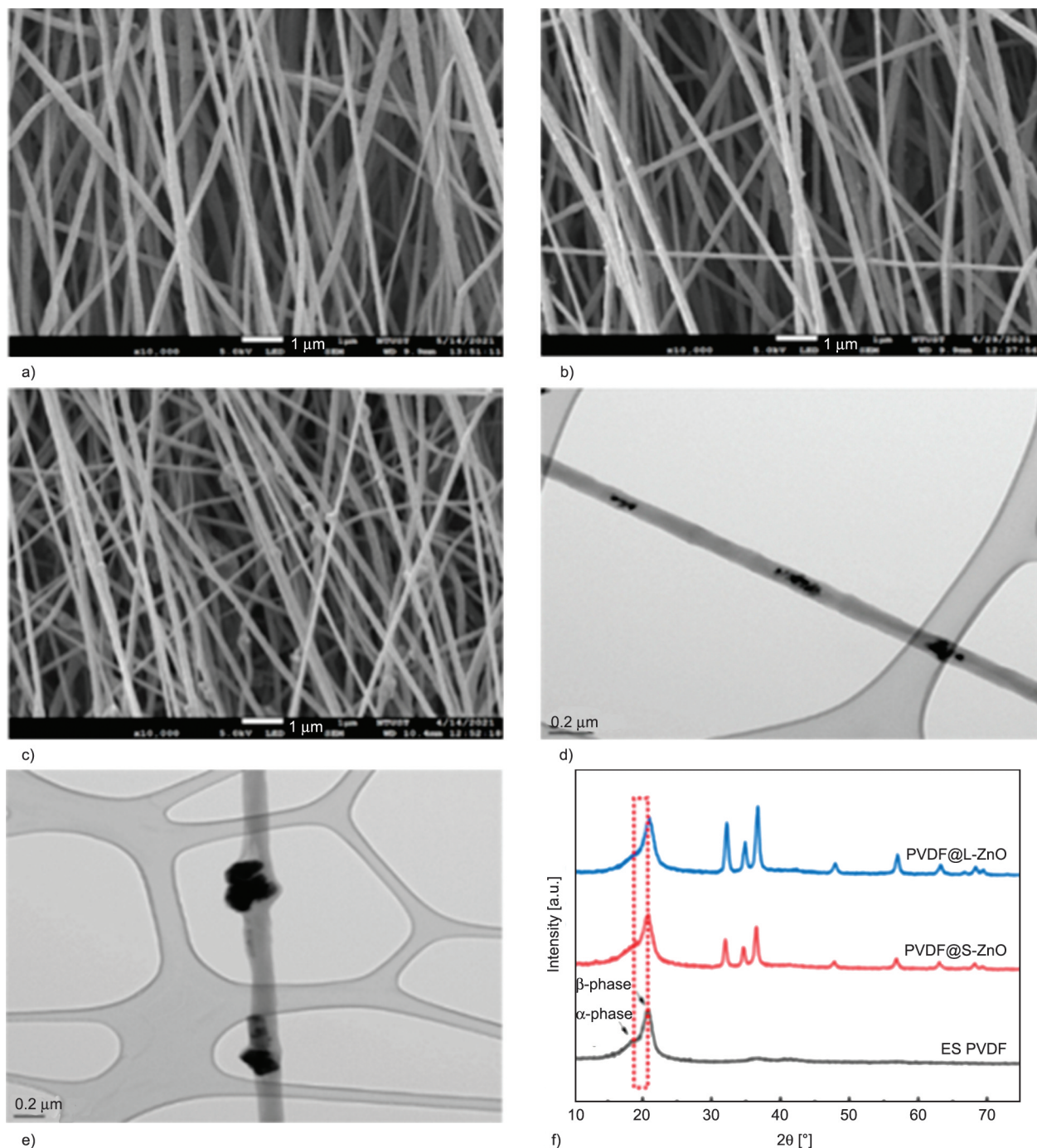
PVDF fibers (Figure 1e). Figure 1f presents the XRD patterns of pure PVDF and PVDF@ZnO nanocomposites. For PVDF, all the diffraction patterns can be ascribed to pure PVDF with JCPDS card numbers of 16–1638 [67], indicating successful preparation of PVDF nanofiber. While the XRD diffraction patterns of both small and large ZnO can be indexed to card number (JCPDS 36-1451) [68]. The nanocomposite with small and large ZnO displayed both characteristics peaks of ZnO and PVDF. Besides, after incorporating ZnO in the PVDF, the relative diffraction intensity peak at two theta angle  $18.6^\circ$  can be ascribed to the reflection of the  $\alpha$  phase at (020) decreased. In contrast, that diffraction peak intensity at  $2\theta$   $20.6^\circ$  that can be indexed to  $\beta$ -phase reflection of PVDF at ((110)/(020)) increased [69, 70]. This result indicates the improvement of  $\beta$ -phase formation of PVDF which is very important for piezoelectric property enhancement in presence of ZnO in general and PVDF@L-ZnO in particular.

Figure 2 shows the FTIR spectra of pure PVDF and PVDF with small and large-particle ZnO. The peaks at 975, 795, and  $765 \text{ cm}^{-1}$  were ascribed to the  $\alpha$ -phase, while the peaks at 1278 and  $840 \text{ cm}^{-1}$  were attributed to the  $\beta$ -phase [66]. After the incorporation of small and large-particle ZnO, the  $\beta$ -phase of PVDF was enhanced, and PVDF@L-ZnO displayed the highest amount of  $\beta$ -phase. The relative  $\beta$ -phase fractions ( $F(\beta)$ ) of the samples were calculated from the FTIR spectra; the absorption is assumed to follow the Beer-Lambert law [66], and  $F(\beta)$  is determined based on Equation (1) as:

$$F(\beta) = \frac{X_\beta}{X_\alpha + X_\beta} = \frac{A_\beta}{\frac{K_\beta}{K_\alpha} A_\alpha + A_\beta} \quad (1)$$

where  $A_\beta$  and  $A_\alpha$  are the ratios of absorbed and incident light intensities at 840 and  $765 \text{ cm}^{-1}$ , respectively.  $K_\beta$  and  $K_\alpha$  are the absorption coefficients at the respective wavenumbers, and  $X_\beta$  and  $X_\alpha$  are the degrees of crystallinity of each phase. The values of  $K_\beta$  and  $K_\alpha$  were  $7.7 \times 10^4$  and  $6.1 \times 10^4 \text{ cm}^2/\text{mol}$ , respectively. Therefore, the constant factor of 1.3 was calculated using the absorption coefficient rate  $K_\beta/K_\alpha$  at the corresponding wavenumber. The results of  $F(\beta)$  of pure PVDF and PVDF@ZnO nanocomposites listed in Table 1 show that incorporating ZnO into the PVDF can effectively increase the  $\beta$ -phase crystallinity of the electrospun PVDF. In particular, ZnO with a large particle size enhanced the relative  $\beta$ -phase fractions from 81 to 91% for ZnO-free electrospun PVDF fiber





**Figure 1.** FESEM images of (a) pure PVDF, (b) PVDF@S-ZnO, (c) PVDF@L-ZnO, (d) TEM images of PVDF@S-ZnO, (e) PVDF@L-ZnO, (f) XRD pattern of pure PVDF and PVDF@S-ZnO, PVDF@L-ZnO.

membranes. This enhanced  $\beta$ -phase formation of PVDF@L-ZnO nanocomposites is due to the induction of charge accumulation by the electrostatic field during the electrospinning process used for sample preparation in this study. The polarization effect caused by the high electrostatic voltage [71] is very pronounced in the larger size ZnO. The larger size of ZnO also played an important role in inducing the  $\beta$ -phase nucleation of PVDF [72]. In addition, the electrical conductivity, which is an important

parameter of piezoelectric performance, also increases with the increase of particle size [73, 74]. Besides, the presence of ZnO can improve the induction of charge accumulation between ZnO and PVDF, further promoting the PVDF chain alignment in the  $\beta$ -phase conformation [66]. In general, polymer crystallization is affected by reinforcements in two different ways: 1) the reinforcement can act as a nucleation site, and 2) it can immobilize polymer chains; polymer chain immobilization delays the crystallization

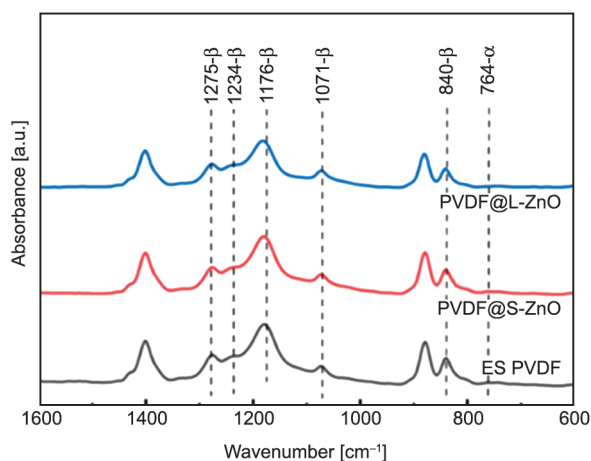


**Figure 2.** FTIR spectra of pure ES PVDF and PVDF@S-ZnO, PVDF@L-ZnO.

**Table 1.** Piezoelectric coefficients and  $F(\beta)\%$  of the synthesized samples.

Sample name	$F(\beta)$ [%]	$d_{33}$ [pC/N]
S-ZnO	–	4.5
L-ZnO	–	8.3
ES PVDF	81	25.3
PVDF@S-ZnO	85	30.4
PVDF@L-ZnO	91	35.2

process, while the reinforcement, which acts as a nucleation site, enhances the crystallinity [44]. Therefore, the incorporation of ZnO influenced the crystallinity of the PVDF. The  $d_{33}$  values listed in Table 1 also indicate that the  $d_{33}$  value of PVDF was significantly enhanced by the incorporation of ZnO nanoparticles, and the highest  $d_{33}$  value was obtained by PVDF@L-ZnO. The value of  $d_{33}$  exhibited by PVDF@L-ZnO (35.2 pC/N) was approximately 1.5 times that of the pure PVDF fiber membrane (25.3 pC/N). Moreover, this high  $d_{33}$  value can be ascribed to the presence of high  $\beta$ -phase nucleation and the combined synergic effect of  $\beta$ -phase crystalline PVDF and piezoelectric ZnO nanoparticles [75]. These findings show that ZnO can: 1) effectively and significantly induce the formation of the  $\beta$ -phase of PVDF [56, 76] and 2) effectively increase  $d_{33}$  owing to a piezoelectric property of ZnO that can directly contribute to its  $d_{33}$ .

### 3.2. Piezoelectric property of PVDF@ZnO PENG device

#### 3.2.1. Piezoelectric mechanism of PVDF@ZnO PENG

The developed PVDF@ZnO fiber membrane with an electrode was sandwiched between two copper

electrodes to efficiently transfer charges. Initially, before a mechanical force is applied to the PVDF@ZnO PENG device, all charges are in their equilibrium state. Thus, there are no potential differences between the copper foils, as shown in Figure 3a. When an external force is applied, the bonds undergo stretching, and a net charge appears owing to the polarization effect, and a fixed charge density exists on the surface in contact with the copper electrodes (Figure 3b). Polarization creates an electric field that is used to convert mechanical energy into electrical energy. Owing to the developed electric field, free charges in the copper electrode move to the end where the fixed charge density possesses an opposite charge, and this flow of charges continues until neutralization of the fixed charge, resulting in a positive voltage, as shown in Figure 3b. When the external stress is released, the polarization disappears, and the free charges in the electrode flow along opposite directions, which results in a negative voltage, as shown in Figure 3c. Finally, the PENG device returns to its original state, and the opposite electrical charges in the copper wires neutralize until it produces zero output voltage, as depicted in Figure 3d.

#### 3.2.2. Piezoelectric response under dynamic compression

The electrical output performances of the developed PENG devices versus the applied compressive force were investigated, and the results are presented in Figure 4. As observed from the result, the PVDF@L-ZnO PENG device exhibited the highest output voltage of 5.6 V under an applied force of 16 N (12.7 kPa), whereas the pure PVDF PENG device exhibited an output voltage of only 4.5 V under the same condition as depicted in Figure 4a. This result shows that the piezoelectric sensitivity of the PVDF can be enhanced by the incorporation of ZnO nanoparticles, and its enhancement is also dependent on the size of the ZnO nanoparticles, where large ZnO nanoparticles lead to high enhancement. This enhancement in the piezoelectric sensitivity is owing to an increase in the  $d_{33}$  of PVDF [77]. The output electrical current was also evaluated, and the result shown in Figure 4b indicates that the PVDF@L-ZnO PENG device generated approximately 1308 nA. However, only 600 nA was produced by PVDF PENG without ZnO nanoparticles. This result reveals that the incorporation of L-ZnO into PVDF can improve the output electrical current by approximately 116% compared to

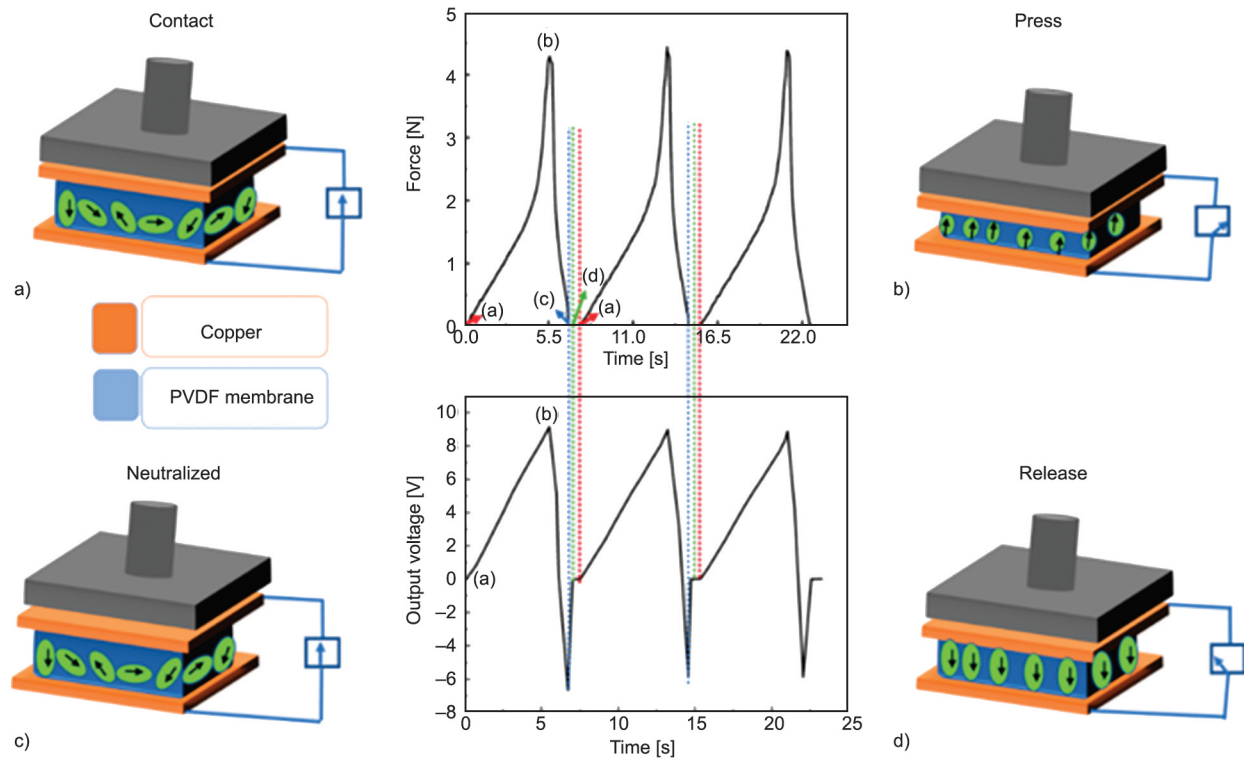


**Figure 3.** Mechanism of PVDF@ZnO PENG (a) normal state of the device, (b) compression of the device due to the applied force and flow of charge in the Cu foils owing to piezoelectric effect, (c) release of applied force and reverse flow of charges, and (d) neutralized state, which is after recovering to the original condition of the device (inset figure of piezo potential generated during this process).

the PENG device composed of pure PVDF. The PVDF@L-ZnO nanocomposite presented better piezoelectric response due to its large  $d_{33}$ , and reduced the contact surface between PVDF and ZnO nanoparticles, resulting in higher piezoelectricity of ZnO@PVDF nanocomposites [58]. The results can be attributed to the smaller interfacial area and higher connectivity of L-ZnO@PVDF nanocomposites, which would lead to higher polarization efficiency than S-ZnO@PVDF nanocomposites. In addition, the larger particle size has high electrical conductivity, which is also critical for piezoelectric performance [73, 74, 78]. These enhancements in the output voltage/current sensitivity indicate the promising potential application of the developed PENG device in different sensor fields. As displayed in Figure 4c, the output voltage increase with the increase in external load resistance, while the output current showed inverse proportionality relationship. The output power that can be generated by the developed PENG devices was also calculated according to the formula ( $P = I^2 R$ ) [79] and the findings in Figure 4d show that our PENG device produced a power density of about  $2160 \mu\text{W}/\text{m}^2$  at a loading resistance of  $10 \text{ M}\Omega$ . The enhancement of the output current, voltage, and

power density by the incorporation of ZnO showed interesting properties of the fabricated PENG device in the field of renewable and green energy harvesting. Therefore, the developed PENG device possesses a promising potential for use as sensor and also in energy harvesting applications. Moreover, the cyclic stability of the developed PENG was also investigated, and the finding in Figure 4e shows that it exhibited outstanding cyclic stability for 5400 cycles with almost no change in output electric voltage. This result indicates the promising candidacy of the fabricated PVDF@L-ZnO PENG device in real application.

Moreover, the electrical output performance of the developed PENG device was compared with that of previously reported PENG devices [54–58]. The results in Table 2 show that the fabricated PVDF@L-ZnO PENG device exhibited better electrical output performance than the previously reported materials.

### 3.2.3 Piezoelectric response under dynamic tension

Figure 5 depicts the stress-strain curve result of pure PVDF and PVDF@ZnO-based PENG devices in which PVDF@L-ZnO presented the highest tensile



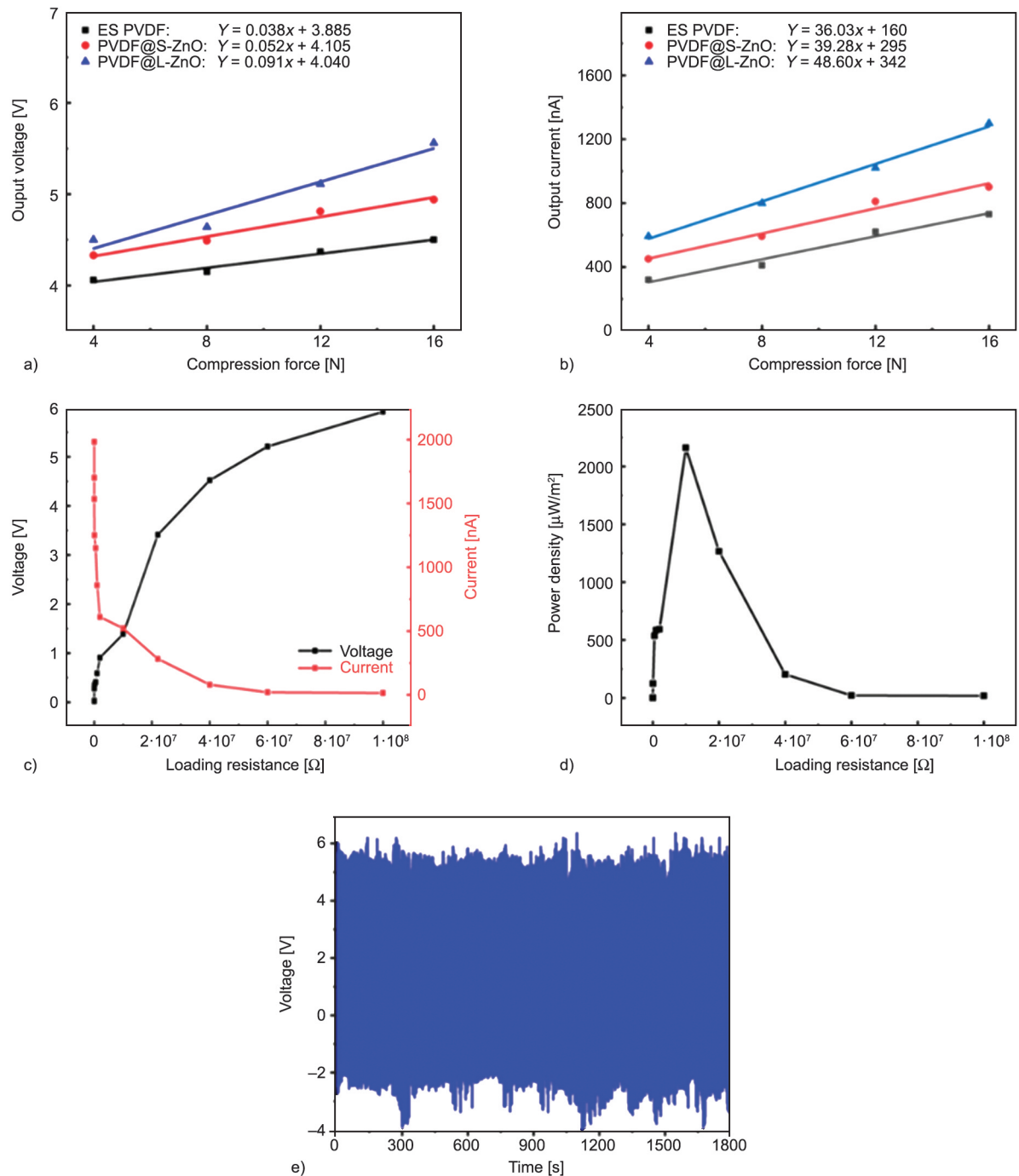


**Figure 4.** Electrical performance of the fabricated PENG device under compression (a) output voltage, and (b) output current (c) load resistance of PVDF@L-ZnO, (d) power density of PVDF@L-ZnO at a compression force of 16 N, and (e) cyclic stability of the developed device.

**Table 2.** Comparison of electrical output performances of different PVDF-based PENG devices with PVDF@L-ZnO PENG device.

Piezoelectric material	Sample size [ $\text{cm}^2$ ]	Peak voltage [V]	Peak current [ $\mu\text{A}$ ]	Force [N]	Power density [ $\mu\text{W}/\text{cm}^2$ ]	References
PVDF/BaTiO <sub>3</sub>	2.60	9.30	0.80	12.00	0.12	[80]
PVDF/BiCl <sub>3</sub>	1.50	1.10	2.00	—	0.20	[81]
PVDF/Fe-ZnO	—	1.10	—	2.50	0.20	[82]
PVDF/ZnO	1.00	0.06	0.03	1.50	0.03	[83]
PVDF@L-ZnO	4.00	5.60	1.31	16.00	0.22	This Work



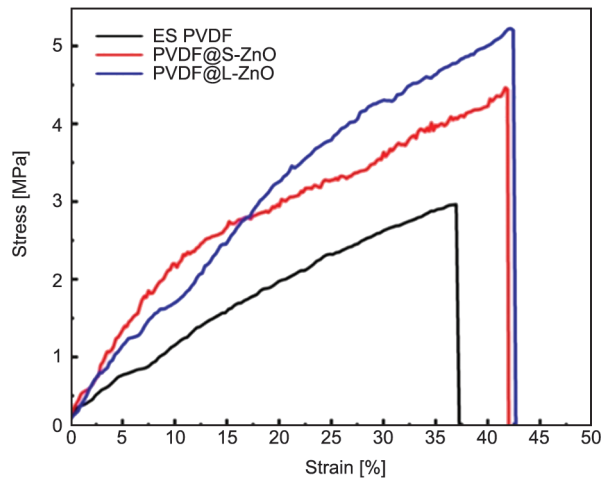


**Figure 5.** Tensile load-displacement curves of electrospun PVDF, PVDF@S-ZnO, and PVDF@L-ZnO.

strength that can be ascribed to strong affinity between ZnO and PVDF [48]. Moreover, the linear part strain value was utilized to determine the testing range since the material can exhibit elastic bounds back properties in the linear range for cyclic testing.

Figure 6a shows that an output voltage and a sensitivity of 42 mV and 10.0 mV/%, respectively, were obtained using a PVDF@L-ZnO PENG, whereas only 9 mV output voltage and 5.5 mV/% sensitivity were achieved using a pure PVDF PENG device. This result shows that the incorporation of large ZnO nanoparticles improves the voltage sensitivity of PVDF by approximately two times. The electrical output current result shown in Figure 6b also shows that an output current of 82 nA was generated by PVDF@ZnO PENG, while the pure PVDF PENG device generated only 45 nA under the same experimental conditions. Moreover, the sensitivity of the developed PVDF@L-ZnO PENG device was about 1.8 times larger than that of pure PVDF PENG. In addition, the linear relationship between the electrical output performance and the percentage of tensile strain demonstrated a linear dependence of the harvested energy on the load or displacement. Figure 6c shows that the electrical output voltage of the PVDF@L-ZnO PENG device increased with increasing external load resistance, according to ohmic laws.

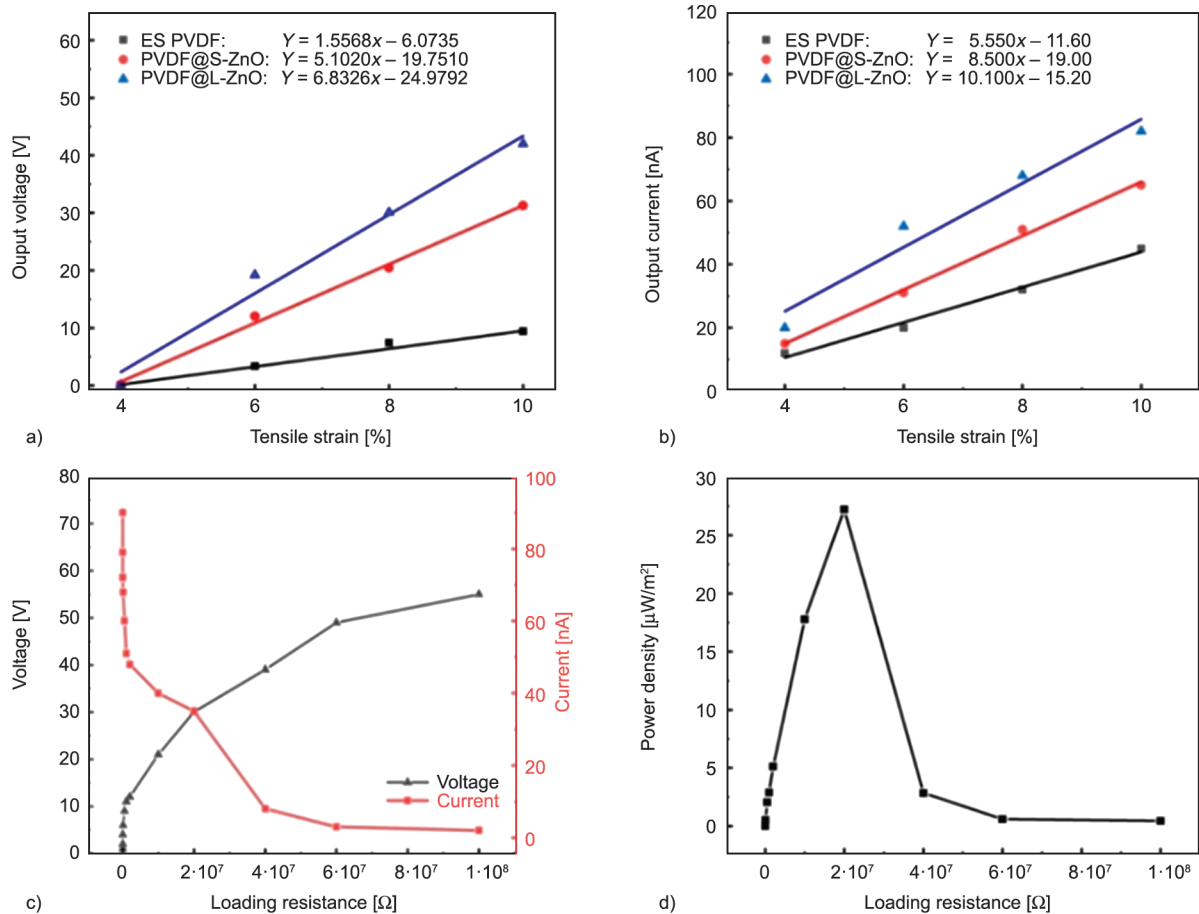


**Figure 6.** (a) Output voltage, (b) output current of electrospun PVDF, PVDF@S-ZnO, and PVDF@L-ZnO under tensile strains from 4 to 10%, (c) load resistance on PVDF@L-ZnO, (d) power density value of PVDF@L-ZnO.

Whereas the electrical output current decreased with increasing external loading resistances. The output power generated by the synthesized PVDF@L-ZnO PENG was also determined, as discussed above, and the result depicted in Figure 6d shows that the device harvested a power density of  $28 \mu\text{W}/\text{m}^2$  at an external loading resistance of  $20 \text{ M}\Omega$ .

### 3.2.4. Piezoelectric response under dynamic bending

Figure 7 displays the piezoelectric output response of the developed PENG devices under bending. The piezoelectric performance of the fabricated PENG was evaluated within the  $0$  to  $180^\circ$  bending angle range, and the piezoelectric performance *versus* bending angle of  $0$  to  $90^\circ$  was provided because the result between  $90$  to  $180^\circ$  is just the reflection of that at the former one [66]. The developed PENG device exhibited an output voltage of  $2.8 \text{ V}$  at a  $90^\circ$  bending angle for the nanocomposite with large ZnO nanoparticles, as presented in Figure 7a whereas an output

voltage of only  $0.8 \text{ V}$  was obtained using a pure PVDF PENG device under the same conditions. This result shows that the output voltage produced by PVDF@L-ZnO PENG was 3.5 times that of pure PVDF. The output current of the fabricated PENG devices was also studied and is displayed in Figure 7b. As observed from the results, the output currents generated by pure PVDF, PVDF@S-ZnO, and PVDF@L-ZnO PENG devices at  $90^\circ$  bending angles were  $150$ ,  $244$ , and  $323 \text{ nA}$ , respectively, under the similar test testing condition. The improvement in output voltage/current indicates that the developed PVDF@L-ZnO PENG device possessed excellent sensitivity under bending conditions and may be utilized as a sensor in flexible and wearable technology. As depicted in Figure 7c, the output voltage increased with an increase in external loading resistance, while the output current displayed an inverse relationship. The output power that can be generated by the developed PENG devices was also calculated, and the result is shown in Figure 7d, in which an output

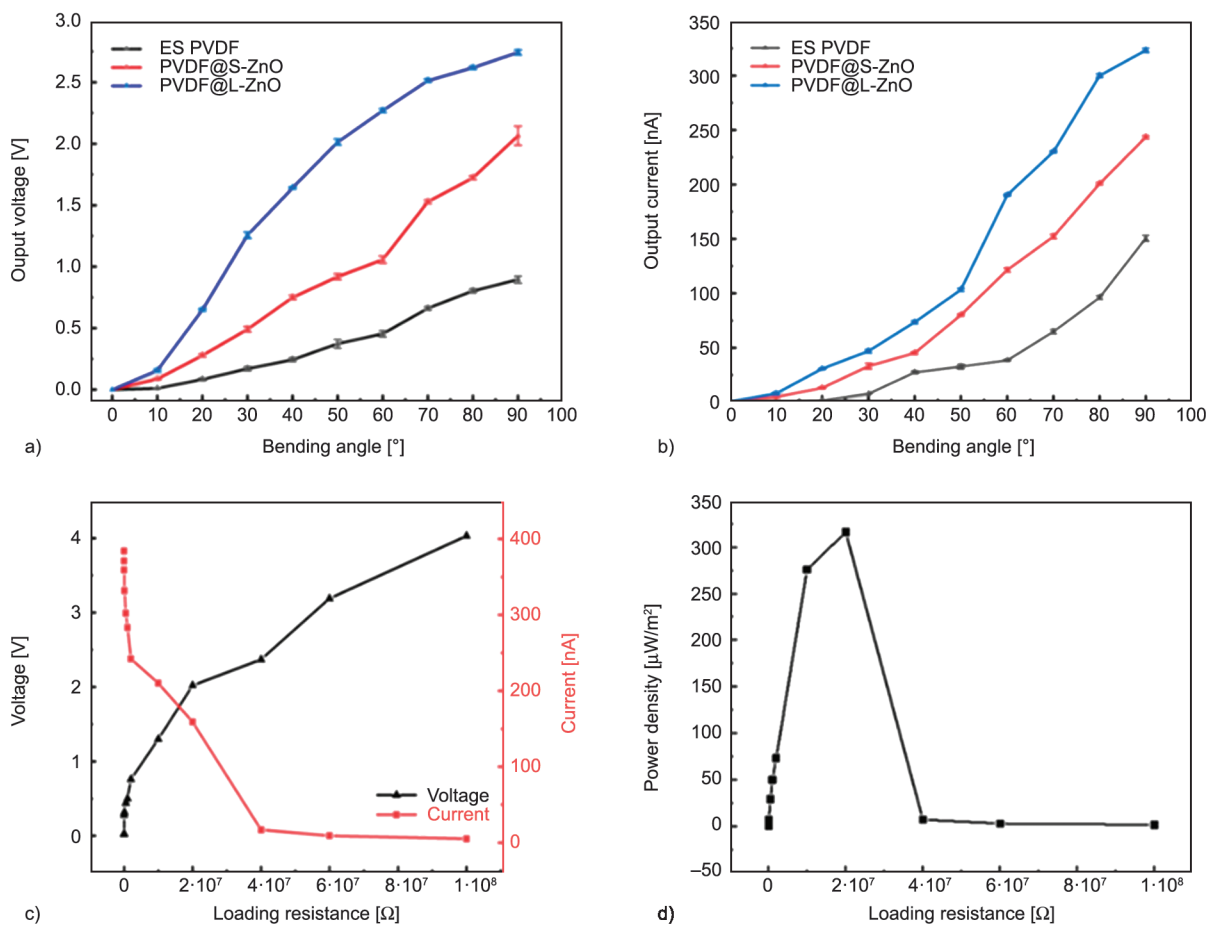


**Figure 7.** Electrical performance of fabricated PNG device under different bending angles, (a) bending angle *versus* output voltage (b) output current of the piezoelectric PVDF samples, (c) load resistance of PVDF@L-ZnO (d) power density of PVDF@L-ZnO under the bending.

power density of  $320 \mu\text{W}/\text{m}^2$  can be produced under a loading resistance of  $20 \text{ M}\Omega$ . These properties show that the developed PVDF@L-ZnO PENG device is capable of harvesting mechanical energy that can be used as a power source [84].

### 3.3. Applications of the developed PENG device

The fabricated PENG device was utilized to harvest energy from body motion and can be used to charge wearable devices to evaluate its applicability in the wearable technology that is gaining attention, and the result is depicted in Figure 8. Figure 8a shows a schematic diagram of the PDVF@L-ZnO PENG device utilized under compression, tensile, and bending conditions from the body movement of the exercising person. The result in Figure 8b shows that the synthesized piezoelectric material harvested an output voltage of approximately 10 V from the body motion (step on it) of a 52 kg person. Furthermore, the

results were also compared with previously developed PENG devices for wearable technology device charging ability, and the results displayed in Table 3 show that the fabricated PVDF@L-ZnO PENG device presented outstanding energy harvesting properties compared to those reported in previous studies [54, 60, 61]. This result shows that the PVDF@L-ZnO PENG device can be successfully applied to wearable technology. Moreover, an electrical output voltage of approximately 0.8 V can also be harvested by the PENG device under tensile stress when stretching is provided by leg movement (Figure 8c). Moreover, the real applicability of the fabricated PVDF@L-ZnO PENG device was extended to harvest energy under bending from body motion while doing regular exercise, and the finding in the Figure 8d depicts that it can generate approximately 1.5 V of electrical output voltage from body movement under bending at  $40\text{--}50^\circ$  angles. These findings indicate the potential applicability of the developed PENG device to

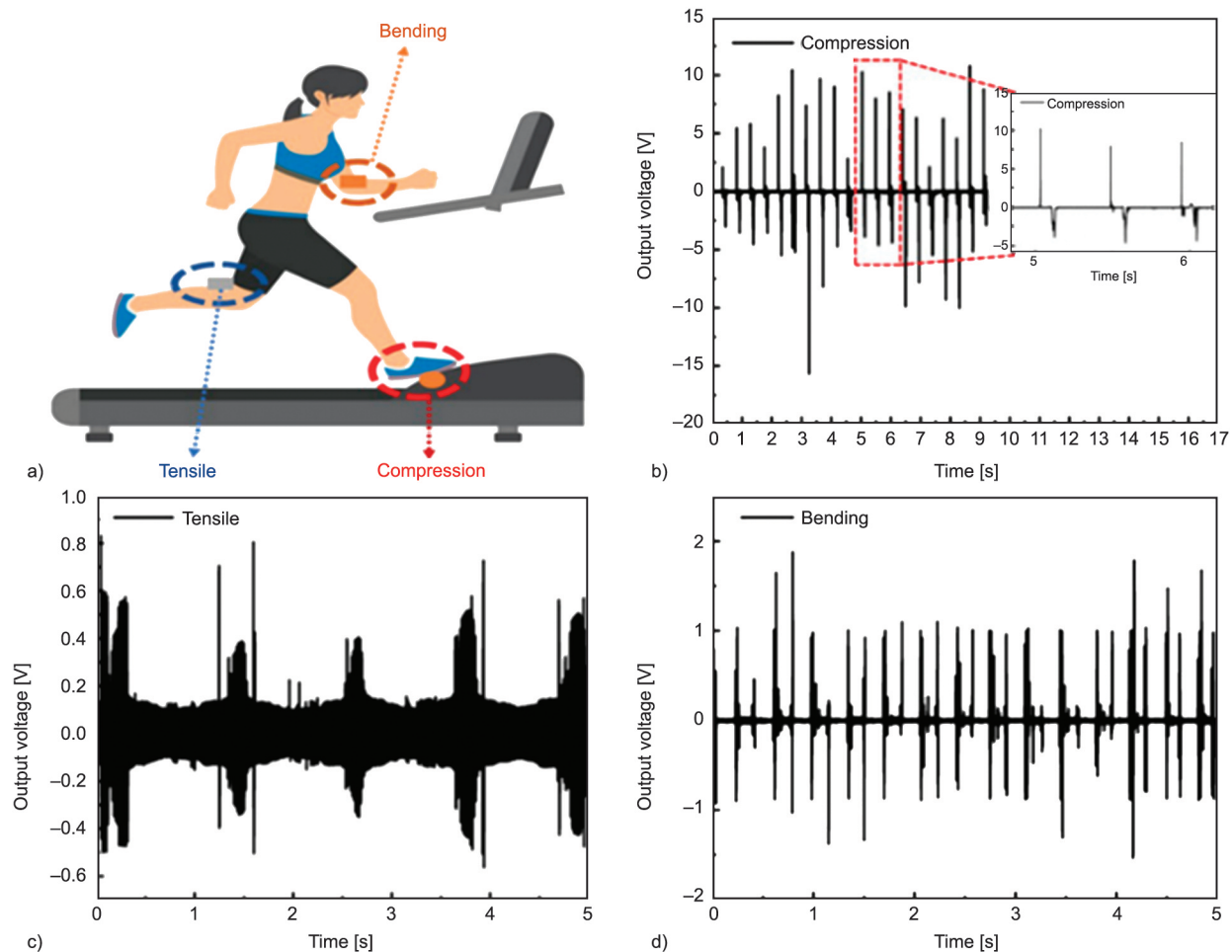


**Figure 8.** (a) The schematic diagram for application of PVDF@L-ZnO in harvesting energy from different body motions, (b) output voltage obtained by walking (compression), (c) output voltage produced by leg stretching (tensile), and (d) output voltage generated by hand bending while doing exercise.

**Table 3.** Comparison of piezoelectric electric properties of different PENG devices in real application energy harvesting from body movement (walking).

PENG device	Device area [cm <sup>2</sup> ]	Output voltage [V]	References
PVDF/TiO <sub>2</sub>	67.50	2.0	[85]
PVDF/BaTiO <sub>3</sub>	5.98	1.0	[80]
PVDF/BNT-ST	35.00	0.7	[86]
PVDF/ZnO	4.00	10.0	This study

scavenge energy from body motion under different conditions, making it a favorable candidate in wearable energy harvesting devices, self-powered sensors, and smart textiles.

The ability of the fabricated PENG device to harvest mechanical energy and convert it to electrical energy in practical applications was also investigated by powering LEDs using hand tapping. The results presented in Figure 9a show that the device transferred mechanical energy derived from hand tapping to electrical energy, which turned on four green LEDs. Herein, we chose four green LEDs to demonstrate the

energy harvesting properties of the developed PENG device under a given loading. The number of LEDs and their brightness can increase with the load and number of PENG devices. A constant DC signal is also required to energize electronic devices with low power. However, PENG devices can generate only AC signals that cannot be used to directly draw electrical signals from energy storage devices. Therefore, the AC output electrical performance generated by the PENG device was rectified utilizing a bridge rectifier circuit to convert it into DC signals. The developed PVDF@L-ZnO PENG was also used to charge capacitors through bridge rectifiers under hand tapping. The capacitor charging result presented in Figure 9b shows that the different capacitors were charged by the developed PENG device, and a smaller capacitor was charged to 1.8 V voltage within 51 s, while a larger capacitor required more time; for example, a 22  $\mu$ F capacitor was charged to the same voltage within 108 s. The amount of energy harvested and stored by the PENG device using the capacitor was

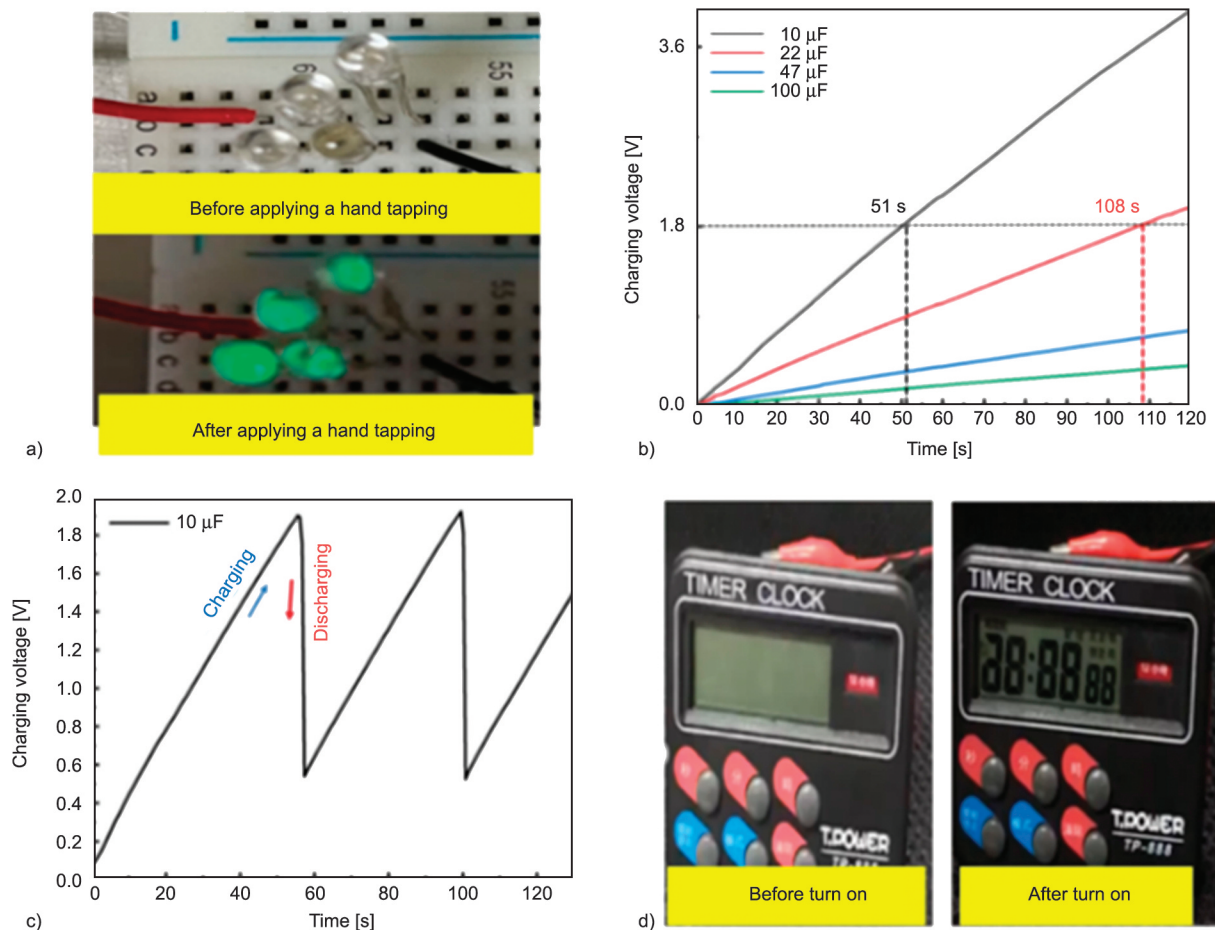


**Figure 9.** Applications of PVDF@L-ZnO PENG device, (a) photographic images of 4 green LEDs (b) capacitor charging voltage, (c) charging to turn on and discharging after turn on stability of a 10  $\mu$ F capacitor under hand tapping, and (d) images of LCD timer clock turned on through a bridge rectifier with 10  $\mu$ F capacitor.



also calculated using the formula  $U_e = 1/2 \cdot C V^2$  where,  $U_e$  is the stored energy,  $C$  is the capacitor capacity, and  $V$  is the generated output voltage [87, 88]. The calculated result indicates that approximately 80  $\mu\text{J}$  of energy was harvested and stored using the developed PENG device within 120 s using a 10  $\mu\text{F}$  capacitor. The amount of energy harvested and stored by the fabricated PVDF@L-ZnO PENG device was also compared with piezoelectric devices in the literature [55, 62, 66, 67], and the results listed in Table 4 show that the developed PVDF@L-ZnO PENG device exhibited better energy harvesting properties than those reported with PENG devices. Moreover, the application of the PENG device was extended to an LCD by hand tapping. Figure 9c shows that the fabricated PENG device exhibited outstanding LCD cycle charging and discharging stability. Figure 9d indicates that the developed device turned on the LCD at 52 s (162 hand taps) and displayed for 1 s. These results reveal that the fabricated piezoelectric device can be utilized in wearable devices (smart textiles) [89], flexible electronics [90], and stretchable and self-chargeable supercapacitors [91].

**Table 4.** Comparison of the energy harvesting and storing property of the PVDF@L-ZnO PNG device with already reported PENG devices.

PENG device	Device area [cm <sup>2</sup> ]	Calculated stored energy [ $\mu\text{J}$ ]	References
PVDF@BCI	2.25	4.9	[81]
BF-PNG	1.95	3.9	[87]
TOCN@MoS <sub>2</sub>	4.50	12.8	[92]
PDMS@BST:La	2.25	1.6	[93]
PVDF@L-ZnO	4.00	80.0	This study

Furthermore, the electric output voltage harvested by the developed PVDF@L-ZnO PENG device by hand tapping was also displayed in Figure 10a, and the result reveals that about 5 V output voltage can be harvested by the device. Besides, the electrical output current that can be generated by our current by hand tapping was evaluated, and the result in Figure 10b indicates that about 1  $\mu\text{A}$  of output electrical current can be produced by the synthesized device under hand tapping. These results reveal that the fabricated piezoelectric device can be used in wearable devices (smart textiles) [89], flexible electronics [90], and stretchable and self-chargeable supercapacitors [91].

### 3.4. Practical applications of the fabricated PENG for daily life energy-harvesting

Different types of machines are used in our daily life, which produces mechanical energy such as vibration energy during their usage. This type of energy is considered as waste energy and harvesting it is crucial. Therefore, the developed PENG device in this study was also applied for harvesting wasted vibration energy from different instruments such as freeze-dryer, centrifuge machines, and air compressors used for normal operation. Harvesting these types of available, wasted, green, and renewable energies is crucial for the increasing energy demand of our world from an economical and environment-friendly perspective. The result presented in Figure 11a shows that the developed PENG device harvested waste mechanical energy from a freeze-dryer being used at a machine operation frequency of 60 Hz and harvested an electrical output voltage of 0.3 V. Figure 11b shows that the PENG device placed on a centrifuge

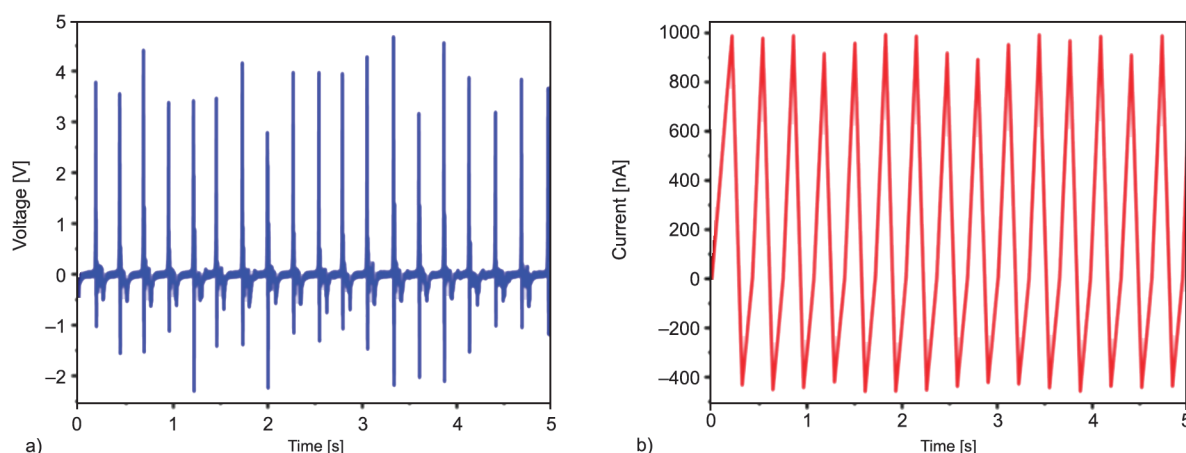


**Figure 10.** Electrical output performances of the developed PVDF@L-ZnO device by hand tapping (a) voltage and (b) current.

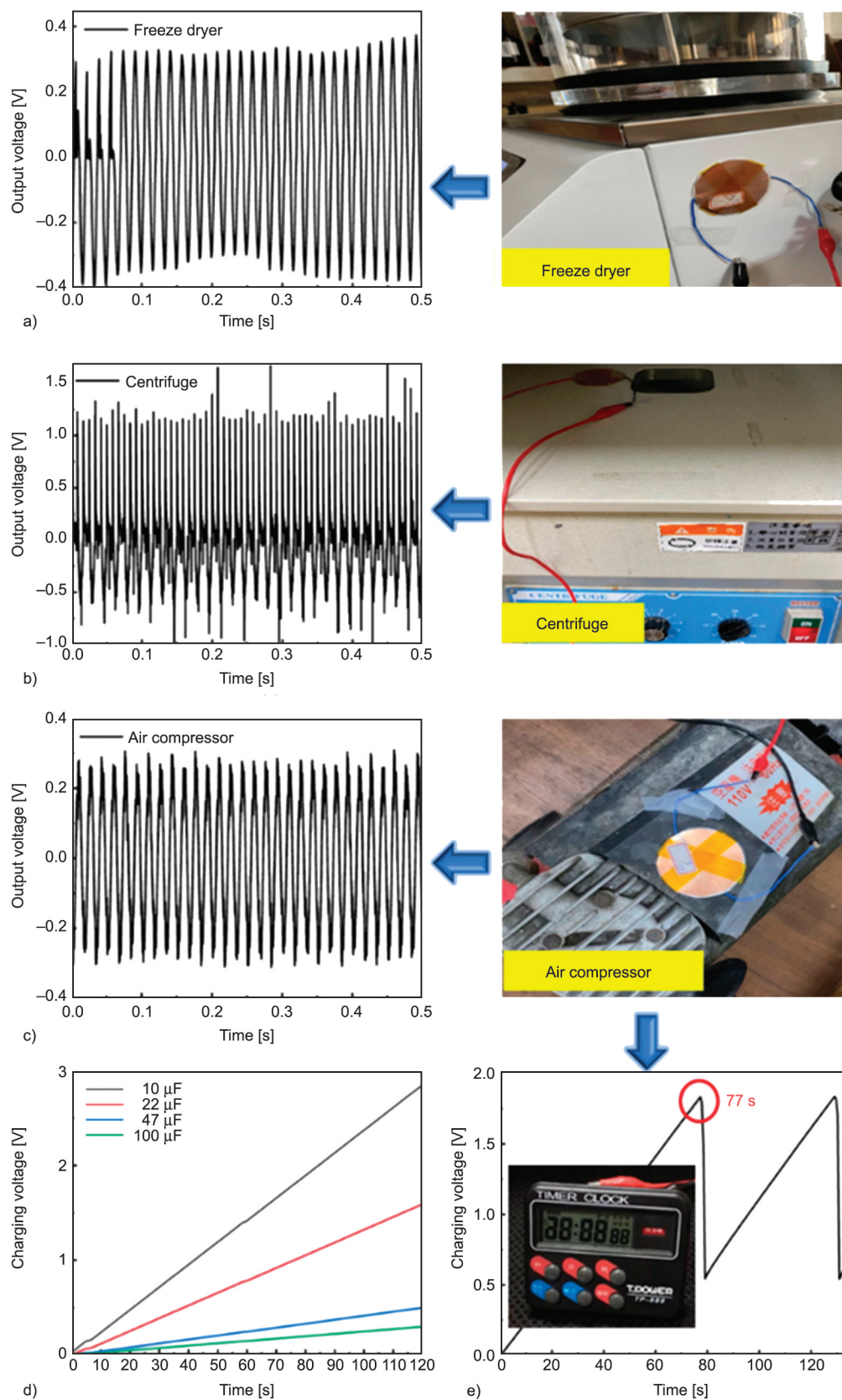


**Figure 11.** Real-time applications of PVDF@L-ZnO PENG device for harvesting waste vibrational mechanical energy. (a) Photographs of freeze dryer and electrical voltage. (b) Photographs of the centrifuge and electrical voltage. (c) Photographs of air compressor and electrical voltage, and (d) various commercial capacitor charging properties of the PENG from waste vibration energy, and (e) LCD turning on after 77 s, and cyclic charging and discharging stability of the PENG device, respectively.

machine being operated at 2400 rpm to harvest the waste vibration energy, and the findings indicate that an electrical output voltage of 1.3 V was harvested using the developed PENG device. Similarly, the result depicted in Figure 11c illustrates that the developed PENG device produced an electrical output voltage of 0.3 V using waste mechanical energy from an air compressor machine used for its usual application. The harvested-waste vibration energy from the centrifuge was used to charge different capacitors and the results (Figure 11d) depict that capacitors of various capacitance were charged by the fabricated PENG device; for instance, a capacitor of 10  $\mu$ F capacitance was charged to 2.9 V within 120 s. The amount of energy that was harvested by the PENG device from waste vibration energy was also calculated, and the obtained result shows that approximately 42  $\mu$ J of wasted vibration energy was harvested within 120 s using the developed PENG device with a 10  $\mu$ F capacitor. The harvested and stored energy is much higher than the minimal external electrical energy (1.1  $\mu$ J) required to trigger the action potential of artificially contracted heart for animals in biomedical applications [94, 95]. Thus, the developed PVDF@L-ZnO device may be used for the fabrication of biomedical sensors and interfacing with human body organs. Among these capacitors, a 10- $\mu$ F capacitor was chosen for turning on the LCD using waste vibration energy harvested from the centrifuge machine, and the result in Figure 11e (inset) shows that the LCD was turned on at 77 for 1 s by the energy harvested from waste vibration. These results indicate the promising applicability of the developed PENG device for harvesting wasted vibration energy, which may enable users to charge their electronic devices while carrying out their normal daily activities [96]. Therefore, we hope that the developed PENG device will play an important role in the utilization of green and renewable energy sources.

#### 4. Conclusions

In this work, electrospun PVDF@ZnO membranes composed of ZnO of different particle sizes were prepared by solution electrospinning, and the effect of the particle size on the piezoelectric properties of the PVDF PENG was systematically investigated. The piezoelectric properties of the fabricated PENG device were evaluated under different mechanical conditions of tension, compression, and bending.

The results indicate that the incorporation of ZnO nanoparticles enhanced the piezoelectric response of PVDF under all the studied conditions. In particular, the PVDF@L-ZnO PENG device generated an electrical output voltage and current of 42 mV and 82 nA, respectively, under tension, 2.8 V and 323 nA, respectively, under bending, as well as 5.6 V and 1308 nA, respectively, under compression. Moreover, it also generated an electrical output voltage of 10 V using the body motion (step on it) of a 52 kg person, 0.8 V when a stretch was provided by leg movement, and 1.5 V under bending while exercising. In addition, the developed PVDF@L-ZnO PENG device showed an interesting waste vibration energy harvesting ability by storing approximately 80  $\mu$ J within 120 s, which makes it a promising candidate for practical applications. The developed PENG device also displayed stable cyclic charging and discharging properties in vibration energy harvesting and played a significant role in the generation of green and renewable energy, which is very important for our environment.

#### Acknowledgements

The authors would like to acknowledge the Ministry of Science and Technology of Taiwan, Republic of China for funding part of this work under contract numbers: MOST 108-2221-E-011-040-MY2 and NTUST-NPUS-NTUST Joint Research Program, under the grant number NPUS-NTUST-NTUST-109-04.

#### References

- [1] Sahatiya P., Kannan S., Badhulika S.: Few layer MoS<sub>2</sub> and *in situ* poled PVDF nanofibers on low cost paper substrate as high performance piezo-triboelectric hybrid nanogenerator: Energy harvesting from handwriting and human touch. *Applied Materials Today*, **13**, 91–99 (2018).  
<https://doi.org/10.1016/j.apmt.2018.08.009>
- [2] Selvaraj A. R., Raja I. S., Chinnadurai D., Rajendiran R., Cho I., Han D-W., Prabakar K.: Electrospun one dimensional (1D) pseudocapacitive nanorods embedded carbon nanofiber as positrode and graphene wrapped carbon nanofiber as negatrode for enhanced electrochemical energy storage. *Journal of Energy Storage*, **46**, 103731 (2022).  
<https://doi.org/10.1016/j.est.2021.103731>
- [3] Gokana M. R., Wu C-M., Reddicherla U., Motora K. G.: Scalable preparation of ultrathin porous polyurethane membrane based triboelectric nanogenerator for mechanical energy harvesting. *Express Polymer Letters*, **15**, 1019–1031 (2021).  
<https://doi.org/10.3144/expresspolymlett.2021.82>



- [4] Son M., Park H., Liu L., Choi H., Kim J. H., Choi H.: Thin-film nanocomposite membrane with CNT positioning in support layer for energy harvesting from saline water. *Chemical Engineering Journal*, **284**, 68–77 (2016).  
<https://doi.org/10.1016/j.cej.2015.08.134>
- [5] Mehrali M., ten Elshof J. E., Shahi M., Mahmoudi A.: Simultaneous solar-thermal energy harvesting and storage via shape stabilized salt hydrate phase change material. *Chemical Engineering Journal*, **405**, 126624 (2021).  
<https://doi.org/10.1016/j.cej.2020.126624>
- [6] Kwak W., Lee Y.: Optimal design and experimental verification of piezoelectric energy harvester with fractal structure. *Applied Energy*, **282**, 116121 (2021).  
<https://doi.org/10.1016/j.apenergy.2020.116121>
- [7] Dhas S. D., Maldar P. S., Patil M. D., Waikar M. R., Sonkawade R. G., Moholkar A. V.: Sol-gel synthesized nickel oxide nanostructures on nickel foam and nickel mesh for a targeted energy storage application. *Journal of Energy Storage*, **47**, 103658 (2021).  
<https://doi.org/10.1016/j.est.2021.103658>
- [8] Kumar S., Saravanan M. P., Kumar D., Venkatesh R.: Screen-printed film deposited using quasi 2-dimensional Bi<sub>2</sub>Se<sub>3</sub> nanostructures for desalination membrane filler application. *Journal of Environmental Chemical Engineering*, **10**, 107128 (2022).  
<https://doi.org/10.1016/j.jece.2022.107128>
- [9] Dewan A., Ay S. U., Karim M. N., Beyenal H.: Alternative power sources for remote sensors: A review. *Journal of Power Sources*, **245**, 129–143 (2014).  
<https://doi.org/10.1016/j.jpowsour.2013.06.081>
- [10] Chamankar N., Khajavi R., Yousefi A. A., Rashidi A., Golestanifard F.: A flexible piezoelectric pressure sensor based on PVDF nanocomposite fibers doped with PZT particles for energy harvesting applications. *Ceramics International*, **46**, 19669–19681 (2020).  
<https://doi.org/10.1016/j.ceramint.2020.03.210>
- [11] Park H.: Solar remediation of wastewater and saline water with concurrent production of value-added chemicals. *Journal of Environmental Chemical Engineering*, **10**, 106919 (2022).  
<https://doi.org/10.1016/j.jece.2021.106919>
- [12] Zhang D., Yang F., Shimotori T., Wang K.-C., Huang Y.: Performance evaluation of power management systems in microbial fuel cell-based energy harvesting applications for driving small electronic devices. *Journal of Power Sources*, **217**, 65–71 (2012).  
<https://doi.org/10.1016/j.jpowsour.2012.06.013>
- [13] Rani G. M., Wu C.-M., Motora K. G., Umapathi R.: Waste-to-energy: Utilization of recycled waste materials to fabricate triboelectric nanogenerator for mechanical energy harvesting. *Journal of Cleaner Production*, **363**, 132532 (2022).  
<https://doi.org/10.1016/j.jclepro.2022.132532>
- [14] Won S. S., Seo H., Kawahara M., Glinsek S., Lee J., Kim Y., Jeong C. K., Kingon A. I., Kim S.-H.: Flexible vibrational energy harvesting devices using strain-engineered perovskite piezoelectric thin films. *Nano Energy*, **55**, 182–192 (2019).  
<https://doi.org/10.1016/j.nanoen.2018.10.068>
- [15] Sun Y., Chen B., Wang F., Zhou S., Wang H.: A novel adaptive control method for a class of stochastic switched pure feedback systems. *Neurocomputing*, **367**, 337–345 (2019).  
<https://doi.org/10.1016/j.neucom.2019.06.061>
- [16] Ippili S., Jella V., Eom J.-H., Kim J., Hong S., Choi J.-S., Tran V.-D., van Hieu N., Kim Y.-J., Kim H.-J., Yoon S.-G.: An eco-friendly flexible piezoelectric energy harvester that delivers high output performance is based on lead-free MASnI<sub>3</sub> films and MASnI<sub>3</sub>-PVDF composite films. *Nano Energy*, **57**, 911–923 (2019).  
<https://doi.org/10.1016/j.nanoen.2019.01.005>
- [17] Yuan Z., Wei X., Jin X., Sun Y., Wu Z., Wang Z. L.: Magnetic energy harvesting of transmission lines by the swinging triboelectric nanogenerator. *Materials Today Energy*, **22**, 100848 (2021).  
<https://doi.org/10.1016/j.mtener.2021.100848>
- [18] Khalili M., Biten A. B., Vishwakarma G., Ahmed S., Papagiannakis A. T.: Electro-mechanical characterization of a piezoelectric energy harvester. *Applied Energy*, **253**, 113585 (2019).  
<https://doi.org/10.1016/j.apenergy.2019.113585>
- [19] Ma D., Lan G., Xu W., Hassan M., Hu W.: Simultaneous energy harvesting and gait recognition using piezoelectric energy harvester. *IEEE Transactions on Mobile Computing*, **21**, 2198–2209 (2020).  
<https://doi.org/10.1109/TMC.2020.3035045>
- [20] Sudevalayam S., Kulkarni P.: Energy harvesting sensor nodes: Survey and implications. *IEEE Communications Surveys and Tutorials*, **13**, 443–461 (2010).  
<https://doi.org/10.1109/SURV.2011.060710.00094>
- [21] La Rosa R., Pandiyan A. Y. S., Trigona C., Andò B., Baglio S.: An integrated circuit to null standby using energy provided by mems sensors. *Acta IMEKO*, **9**, 144–150 (2020).  
[https://doi.org/10.21014/acta\\_imeko.v9i4.741](https://doi.org/10.21014/acta_imeko.v9i4.741)
- [22] Xiong H., Wang L.: Piezoelectric energy harvester for public roadway: On-site installation and evaluation. *Applied Energy*, **174**, 101–107 (2016).  
<https://doi.org/10.1016/j.apenergy.2016.04.031>
- [23] Wang S., Wang C., Yu G., Gao Z.: Development and performance of a piezoelectric energy conversion structure applied in pavement. *Energy Conversion and Management*, **207**, 112571 (2020).  
<https://doi.org/10.1016/j.enconman.2020.112571>
- [24] Wang J., Zhao B., Liao W.-H., Liang J.: New insight into piezoelectric energy harvesting with mechanical and electrical nonlinearities. *Smart Materials and Structures*, **29**, 04LT01 (2020).  
<https://doi.org/10.1088/1361-665x/ab7543>



- [25] He F.-A., Kim M.-J., Chen S.-M., Wu Y.-S., Lam K.-H., Chan H. L.-W., Fan J.-T.: Tough and porous piezoelectric P(VDF-TRFE)/organosilicate composite membrane. *High Performance Polymers*, **29**, 133–140 (2017).  
<https://doi.org/10.1177/0954008316631611>
- [26] Cho Y., Jeong J., Choi M., Baek G., Park S., Choi H., Ahn S., Cha S., Kim T., Kang D.-S., Bae J., Park J.-J.: BaTiO<sub>3</sub>@PVDF-TRFE nanocomposites with efficient orientation prepared *via* phase separation nano-coating method for piezoelectric performance improvement and application to 3D-peng. *Chemical Engineering Journal*, **427**, 131030 (2022).  
<https://doi.org/10.1016/j.cej.2021.131030>
- [27] Howells C. A.: Piezoelectric energy harvesting. *Energy Conversion and Management*, **50**, 1847–1850 (2009).  
<https://doi.org/10.1016/j.enconman.2009.02.020>
- [28] Fan K., Chang J., Chao F., Pedrycz W.: Design and development of a multipurpose piezoelectric energy harvester. *Energy Conversion and Management*, **96**, 430–439 (2015).  
<https://doi.org/10.1016/j.enconman.2015.03.014>
- [29] Martins P., Lasheras A., Gutiérrez J., Barandiarán J. M., Orue I., Lanceros-Méndez S.: Optimizing piezoelectric and magnetoelectric responses on CoFe<sub>2</sub>O<sub>4</sub>/P(VDF-TrFE) nanocomposites. *Journal of Physics D: Applied Physics*, **44**, 495303 (2011).  
<https://doi.org/10.1088/0022-3727/44/49/495303>
- [30] Wu C. M., Chou M. H.: Polymorphism, piezoelectricity and sound absorption of electrospun PVDF membranes with and without carbon nanotubes. *Composites Science and Technology*, **127**, 127–133 (2016).  
<https://doi.org/10.1016/j.compscitech.2016.03.001>
- [31] Lee S. H., Choi Y. C., Kim M. S., Ryu K. M., Jeong Y. G.: Fabrication and characterization of piezoelectric composite nanofibers based on poly(vinylidene fluoride-co-hexafluoropropylene) and barium titanate nanoparticle. *Fibers and Polymers*, **21**, 473–479 (2020).  
<https://doi.org/10.1007/s12221-020-9803-1>
- [32] Guo H., Wu Q., Sun H., Liu X., Sui H.: Organic phosphonic acid-modified BaTiO<sub>3</sub>/P(VDF-TRFE) composite with high output in both voltage and power for flexible piezoelectric nanogenerators. *Materials Today Energy*, **17**, 100489 (2020).  
<https://doi.org/10.1016/j.mtener.2020.100489>
- [33] Singh B., Padha B., Verma S., Satapathi S., Gupta V., Arya S.: Recent advances, challenges, and prospects of piezoelectric materials for self-charging supercapacitor. *Journal of Energy Storage*, **47**, 103547 (2021).  
<https://doi.org/10.1016/j.est.2021.103547>
- [34] Dai B., Huang H., Wang F., Lu C., Kou J., Wang L., Xu Z.: Flowing water enabled piezoelectric potential of flexible composite film for enhanced photocatalytic performance. *Chemical Engineering Journal*, **347**, 263–272 (2018).  
<https://doi.org/10.1016/j.cej.2018.04.008>
- [35] Song G. J., Kim K.-B., Cho J. Y., Woo M. S., Ahn J. H., Eom J. H., Ko S. M., Yang C. H., Hong S. D., Jeong S. Y., Hwang W. S., Woo S. B., Jhun J. P., Jeon D. H., Sung T. H.: Performance of a speed bump piezoelectric energy harvester for an automatic cellphone charging system. *Applied Energy*, **247**, 221–227 (2019).  
<https://doi.org/10.1016/j.apenergy.2019.04.040>
- [36] Parida K., Bhavanasi V., Kumar V., Wang J., Lee P. S.: Fast charging self-powered electric double layer capacitor. *Journal of Power Sources*, **342**, 70–78 (2017).  
<https://doi.org/10.1016/j.jpowsour.2016.11.083>
- [37] Pei J., Zhao Z., Li X., Liu H., Li R.: Effect of preparation techniques on structural and electrical properties of PZT/PVDF composites. *Materials Express*, **7**, 180–188 (2017).  
<https://doi.org/10.1166/mex.2017.1369>
- [38] Kumar V., Park S., Parida K., Bhavanasi V., Lee P. S.: Multi-responsive supercapacitors: Smart solution to store electrical energy. *Materials Today Energy*, **4**, 41–57 (2017).  
<https://doi.org/10.1016/j.mtener.2017.03.004>
- [39] Kim G. H., Hong S. M., Seo Y.: Piezoelectric properties of poly(vinylidene fluoride) and carbon nanotube blends:  $\beta$ -phase development. *Physical Chemistry Chemical Physics*, **11**, 10506–10512 (2009).  
<https://doi.org/10.1039/B912801H>
- [40] Hartono A., Darwin, Ramli, Satira S., Djamal M., Herman: Electric field poling 2G V/m to improve piezoelectricity of PVDF thin film. *AIP Conference Proceedings*, **1719**, 030021 (2016).  
<https://doi.org/10.1063/1.4943716>
- [41] Wu L., Yuan W., Nakamura T., Atobe S., Hu N., Fukunaga H., Chang C., Zemba Y., Li Y., Watanabe T., Liu Y., Alamus, Ning H., Li J., Cui H., Zhang Y.: Enhancement of PVDF's piezoelectricity by VGCF and MWNT. *Advanced Composite Materials*, **22**, 49–63 (2013).  
<https://doi.org/10.1080/09243046.2013.764780>
- [42] Layek R. K., Samanta S., Chatterjee D. P., Nandi A. K.: Physical and mechanical properties of poly(methyl methacrylate) – functionalized graphene/poly(vinylidene fluoride) nanocomposites: Piezoelectric  $\beta$  polymorph formation. *Polymer*, **51**, 5846–5856 (2010).  
<https://doi.org/10.1016/j.polymer.2010.09.067>
- [43] El Achaby M., Arrakhiz F. Z., Vaudreuil S., Essassi E. M., Qaiss A.: Piezoelectric  $\beta$ -polymorph formation and properties enhancement in graphene oxide – PVDF nanocomposite films. *Applied Surface Science*, **258**, 7668–7677 (2012).  
<https://doi.org/10.1016/j.apsusc.2012.04.118>
- [44] Issa A. A., Al-Maadeed M. A., Luyt A. S., Ponnammam D., Hassan M. K.: Physico-mechanical, dielectric, and piezoelectric properties of PVDF electrospun mats containing silver nanoparticles. *C – Journal of Carbon Research*, **3**, 30 (2017).  
<https://doi.org/10.3390/c3040030>

- [45] Motamedi A. S., Mirzadeh H., Hajiesmaeilbaigi F., Bagheri-Khoulenjani S., Shokrgozar M. A.: Piezoelectric electrospun nanocomposite comprising au NPs/PVDF for nerve tissue engineering. *Journal of Biomedical Materials Research Part A*, **105**, 1984–1993 (2017). <https://doi.org/10.1002/jbm.a.36050>
- [46] Chang J., Shen Y., Chu X., Zhang X., Song Y., Lin Y., Nan C-W., Li L.: Large  $d_{33}$  and enhanced ferroelectric/dielectric properties of poly(vinylidene fluoride)-based composites filled with  $\text{Pb}(\text{Zr}_{0.52}\text{Ti}_{0.48})\text{O}_3$  nanofibers. *RSC Advances*, **5**, 51302–51307 (2015). <https://doi.org/10.1039/C5RA07932B>
- [47] Vacche S. D., Oliveira F., Leterrier Y., Michaud V., Damjanovic D., Manson J-A. E.: The effect of processing conditions on the morphology, thermomechanical, dielectric, and piezoelectric properties of P(VDF-TRFE)/ $\text{BaTiO}_3$  composites. *Journal of Materials Science*, **47**, 4763–4774 (2012). <https://doi.org/10.1007/s10853-012-6362-x>
- [48] Jahan N., Mighri F., Rodrigue D., Ajji A.: Synergistic improvement of piezoelectric properties of PVDF/ $\text{CaCO}_3$ /montmorillonite hybrid nanocomposites. *Applied Clay Science*, **152**, 93–100 (2018). <https://doi.org/10.1016/j.clay.2017.10.036>
- [49] Kumar B., Kim S-W.: Energy harvesting based on semiconducting piezoelectric ZnO nanostructures. *Nano Energy*, **1**, 342–355 (2012). <https://doi.org/10.1016/j.nanoen.2012.02.001>
- [50] Xu C., Pan C., Liu Y., Wang Z. L.: Hybrid cells for simultaneously harvesting multi-type energies for self-powered micro/nanosystems. *Nano Energy*, **1**, 259–272 (2012). <https://doi.org/10.1016/j.nanoen.2012.01.002>
- [51] Senasu T., Chankhanittha T., Hemavibool K., Nanan S.: Visible-light-responsive photocatalyst based on ZnO/ $\text{CdS}$  nanocomposite for photodegradation of reactive red azo dye and ofloxacin antibiotic. *Materials Science in Semiconductor Processing*, **123**, 105558 (2021). <https://doi.org/10.1016/j.mssp.2020.105558>
- [52] Meng F., Shi X., Yuan Z., Ji H., Qin W., Shen Y., Xing C.: Detection of four alcohol homologue gases by ZnO gas sensor in dynamic interval temperature modulation mode. *Sensors and Actuators B: Chemical*, **350**, 130867 (2022). <https://doi.org/10.1016/j.snb.2021.130867>
- [53] Lupan O., Magariu N., Khaledialidusti R., Mishra A. K., Hansen S., Krüger H., Postica V., Heinrich H., Viana B., Ono L. K., Cuenya B. R., Chow L., Adelung R., Pauporté T.: Comparison of thermal annealing versus hydrothermal treatment effects on the detection performances of ZnO nanowires. *ACS Applied Materials and Interfaces*, **13**, 10537–10552 (2021). <https://doi.org/10.1021/acsami.0c19170>
- [54] Wang R., Liu S., Liu C. R., Wu W.: Data-driven learning of process–property–performance relation in laser-induced aqueous manufacturing and integration of ZnO piezoelectric nanogenerator for self-powered nanosensors. *Nano Energy*, **83**, 105820 (2021). <https://doi.org/10.1016/j.nanoen.2021.105820>
- [55] Sun B., Li X., Zhao R., Ji H., Qiu J., Zhang N., He D., Wang C.: Electrospun poly(vinylidene fluoride)-zinc oxide hierarchical composite fiber membrane as piezoelectric acoustoelectric nanogenerator. *Journal of Materials Science*, **54**, 2754–2762 (2019). <https://doi.org/10.1007/s10853-018-2985-x>
- [56] Li Z., Zhang X., Li G.: *In situ* ZnO nanowire growth to promote the PVDF piezo phase and the ZnO–PVDF hybrid self-rectified nanogenerator as a touch sensor. *Physical Chemistry Chemical Physics*, **16**, 5475–5479 (2014). <https://doi.org/10.1039/C3CP54083A>
- [57] Lee M., Chen C-Y., Wang S., Cha S. N., Park Y. J., Kim J. M., Chou L-J., Wang Z. L.: A hybrid piezoelectric structure for wearable nanogenerators. *Advanced Materials*, **24**, 1759–1764 (2012). <https://doi.org/10.1002/adma.201200150>
- [58] Chaipanich A.: Effect of PZT particle size on dielectric and piezoelectric properties of PZT–cement composites. *Current Applied Physics*, **7**, 574–577 (2007). <https://doi.org/10.1016/j.cap.2006.11.036>
- [59] Arjun Hari M., Rajan L., Subash C. K., Varghese S.: Effect of nanoparticle size on the piezoelectric properties of PVDF based nanocomposite thin films. *Materials Today: Proceedings*, **46**, 5781–5784 (2021). <https://doi.org/10.1016/j.matpr.2021.02.715>
- [60] Rujijanagul G., Jompruan S., Chaipanich A.: Influence of graphite particle size on electrical properties of modified PZT–polymer composites. *Current Applied Physics*, **8**, 359–362 (2008). <https://doi.org/10.1016/j.cap.2007.10.031>
- [61] Chaipanich A., Jaitanong N.: Effect of PZT particle size on the electromechanical coupling coefficient of 0-3 PZT-cement composites. *Ferroelectrics Letters Section*, **36**, 37–44 (2009). <https://doi.org/10.1080/07315170902938162>
- [62] Chitra, Singh K. C.: Enhanced electrical activity induced by high-energy milling in lead-free BCST piezoceramics. *Materials Letters*, **256**, 126664 (2019). <https://doi.org/10.1016/j.matlet.2019.126664>
- [63] Hunpratub S., Yamwong T., Srilomsak S., Maensiri S., Chindaprasit P.: Effect of particle size on the dielectric and piezoelectric properties of 0–3BCTZO/cement composites. *Ceramics International*, **40**, 1209–1213 (2014). <https://doi.org/10.1016/j.ceramint.2013.05.118>
- [64] Yoon M-S., Khansur N. H., Choi B-K., Lee Y-G., Ur S-C.: The effect of nano-sized BNBT on microstructure and dielectric/piezoelectric properties. *Ceramics International*, **35**, 3027–3036 (2009). <https://doi.org/10.1016/j.ceramint.2009.04.016>

- [65] Li Z., Zhang D., Wu K.: Cement-based 0-3 piezoelectric composites. *Journal of the American Ceramic Society*, **85**, 305–313 (2002).  
<https://doi.org/10.1111/j.1151-2916.2002.tb00089.x>
- [66] Wu C.-M., Chou M.-H., Zeng W.-Y.: Piezoelectric response of aligned electrospun polyvinylidene fluoride/carbon nanotube nanofibrous membranes. *Nanomaterials*, **8**, 420 (2018).  
<https://doi.org/10.3390/nano8060420>
- [67] Nidhi, Patel S., Kumar R.: Synthesis and characterization of magnesium ion conductivity in PVDF based nanocomposite polymer electrolytes disperse with MgO. *Journal of Alloys and Compounds*, **789**, 6–14 (2019)  
<https://doi.org/10.1016/j.jallcom.2019.03.089>
- [68] Yang Z., Ye Z., Xu Z., Zhao B.: Effect of the morphology on the optical properties of ZnO nanostructures. *Physica E: Low-dimensional Systems and Nanostructures*, **42**, 116–119 (2009).  
<https://doi.org/10.1016/j.physe.2009.09.010>
- [69] Wu C.-M., Chou M.-H., Chala T. F., Shimamura Y., Murakami R.-I.: Infrared-driven poly(vinylidene difluoride)/tungsten oxide pyroelectric generator for non-contact energy harvesting. *Composites Science and Technology*, **178**, 26–32 (2019).  
<https://doi.org/10.1016/j.compscitech.2019.05.004>
- [70] Lei T., Yu L., Zheng G., Wang L., Wu D., Sun D.: Electrospinning-induced preferred dipole orientation in PVDF fibers. *Journal of Materials Science*, **50**, 4342–4347 (2015).  
<https://doi.org/10.1007/s10853-015-8986-0>
- [71] Shao H., Fang J., Wang H., Lin T.: Effect of electrospinning parameters and polymer concentrations on mechanical-to-electrical energy conversion of randomly-oriented electrospun poly(vinylidene fluoride) nanofiber mats. *RSC Advances*, **5**, 14345–14350 (2015).  
<https://doi.org/10.1039/C4RA16360E>
- [72] Gonçalves R., Martins P., Correia D. M., Sencadas V., Vilas J., Leon L., Botelho G., Lanceros-Méndez S.: Development of magnetoelectric CoFe<sub>2</sub>O<sub>4</sub>/poly(vinylidene fluoride) microspheres. *RSC Advances*, **5**, 35852–35857 (2015).  
<https://doi.org/10.1039/c5ra04409j>
- [73] Parvez Ahmad M. D., Venkateswara Rao A., Suresh Babu K., Narsinga Rao G.: Particle size effect on the dielectric properties of ZnO nanoparticles. *Materials Chemistry and Physics*, **224**, 79–84 (2019).  
<https://doi.org/10.1016/j.matchemphys.2018.12.002>
- [74] Chen B.-H., Wang B.-W., Gao P.-Z., Zhang P., Chen H.-H.: Effects of raw particle size and annealing on microstructure, electrical and mechanical behaviors of ZnO-based varistors. *Journal of Alloys and Compounds*, **872**, 159638 (2021).  
<https://doi.org/10.1016/j.jallcom.2021.159638>
- [75] Thakur P., Kool A., Hoque N. A., Bagchi B., Khatun F., Biswas P., Brahma D., Roy S., Banerjee S., Das S.: Superior performances of *in situ* synthesized ZnO/PVDF thin film based self-poled piezoelectric nanogenerator and self-charged photo-power bank with high durability. *Nano Energy*, **44**, 456–467 (2018).  
<https://doi.org/10.1016/j.nanoen.2017.11.065>
- [76] Wu C. M., Chou M. H.: Acoustic-electric conversion and piezoelectric properties of electrospun polyvinylidene fluoride/silver nanofibrous membranes. *Express Polymer Letters*, **14**, 103–114 (2020).  
<https://doi.org/10.3144/expresspolymlett.2020.10>
- [77] Han J., Li D., Zhao C., Wang X., Li J., Wu X.: Highly sensitive impact sensor based on PVDF-TRFE/nano-ZnO composite thin film. *Sensors*, **19**, 830 (2019).  
<https://doi.org/10.3390/s19040830>
- [78] Huang S., Lu L., Chang J., Xu D., Liu F., Cheng X.: Influence of ceramic particle size on piezoelectric properties of cement-based piezoelectric composites. *Ferroelectrics*, **332**, 187–194 (2006).  
<https://doi.org/10.1080/00150190600732520>
- [79] Briscoe J., Jalali N., Woolliams P., Stewart M., Weaver P. M., Cain M., Dunn S.: Measurement techniques for piezoelectric nanogenerators. *Energy and Environmental Science*, **6**, 3035–3045 (2013).  
<https://doi.org/10.1039/C3EE41889H>
- [80] Yang Y., Pan H., Xie G., Jiang Y., Chen C., Su Y., Wang Y., Tai H.: Flexible piezoelectric pressure sensor based on polydopamine-modified BaTiO<sub>3</sub>/PVDF composite film for human motion monitoring. *Sensors and Actuators A: Physical*, **301**, 111789 (2020).  
<https://doi.org/10.1016/j.sna.2019.111789>
- [81] Chen C., Bai Z., Cao Y., Dong M., Jiang K., Zhou Y., Tao Y., Gu S., Xu J., Yin X., Xu W.: Enhanced piezoelectric performance of BiCl<sub>3</sub>/PVDF nanofibers-based nanogenerators. *Composites Science and Technology*, **192**, 108100 (2020).  
<https://doi.org/10.1016/j.compscitech.2020.108100>
- [82] Parangusan H., Ponnammam D., AlMaadeed M. A. A.: Investigation on the effect of  $\gamma$ -irradiation on the dielectric and piezoelectric properties of stretchable PVDF/Fe–ZnO nanocomposites for self-powering devices. *Soft Matter*, **14**, 8803–8813 (2018).  
<https://doi.org/10.1039/C8SM01655K>
- [83] Mansouri S., Sheikholeslami T. F., Behzadmehr A.: Investigation on the electrospun PVDF/NP-ZnO nanofibers for application in environmental energy harvesting. *Journal of Materials Research and Technology*, **8**, 1608–1615 (2019).  
<https://doi.org/10.1016/j.jmrt.2018.07.024>
- [84] Wang S., Ding L., Wang Y., Gong X.: Multifunctional triboelectric nanogenerator towards impact energy harvesting and safeguards. *Nano Energy*, **59**, 434–442 (2019).  
<https://doi.org/10.1016/j.nanoen.2019.02.060>

- [85] Alam M. M., Sultana A., Mandal D.: Biomechanical and acoustic energy harvesting from TiO<sub>2</sub> nanoparticle modulated PVDF nanofiber made high performance nanogenerator. *ACS Applied Energy Materials*, **1**, 3103–3112 (2018).  
<https://doi.org/10.1021/acsaem.8b00216>
- [86] Ji S. H., Cho Y-S., Yun J. S.: Wearable core-shell piezoelectric nanofiber yarns for body movement energy harvesting. *Nanomaterials*, **9**, 555 (2019).  
<https://doi.org/10.3390/nano9040555>
- [87] Hanani Z., Izanjar I., Amjoud M., Mezzane D., Lahcini M., Uršič H., Prah U., Saadouni I., El Marssi M., Luk'yanchuk I. A., Kutnjak Z., Gouné M.: Lead-free nanocomposite piezoelectric nanogenerator film for biomechanical energy harvesting. *Nano Energy*, **81**, 105661 (2021).  
<https://doi.org/10.1016/j.nanoen.2020.105661>
- [88] Gokana M. R., Wu C-M., Motora K. G., Qi J. Y., Yen W-T.: Effects of patterned electrode on near infrared light-triggered cesium tungsten bronze/poly(vinylidene)fluoride nanocomposite-based pyroelectric nanogenerator for energy harvesting. *Journal of Power Sources*, **536**, 231524 (2022).  
<https://doi.org/10.1016/j.jpowsour.2022.231524>
- [89] Zhou X., Parida K., Halevi O., Liu Y., Xiong J., Magdassi S., Lee P. S.: All 3D-printed stretchable piezoelectric nanogenerator with non-protruding kirigami structure. *Nano Energy*, **72**, 104676 (2020).  
<https://doi.org/10.1016/j.nanoen.2020.104676>
- [90] Jiang Q., Wu C., Wang Z., Wang A. C., He J-H., Wang Z. L., Alshareef H. N.: MXene electrochemical micro-supercapacitor integrated with triboelectric nanogenerator as a wearable self-charging power unit. *Nano Energy*, **45**, 266–272 (2018).  
<https://doi.org/10.1016/j.nanoen.2018.01.004>
- [91] Zhou D., Wang N., Yang T., Wang L., Cao X., Wang Z. L.: A piezoelectric nanogenerator promotes highly stretchable and self-chargeable supercapacitors. *Materials Horizons*, **7**, 2158–2167 (2020).  
<https://doi.org/10.1039/D0MH00610F>
- [92] Wu T., Song Y., Shi Z., Liu D., Chen S., Xiong C., Yang Q.: High-performance nanogenerators based on flexible cellulose nanofibril/MoS<sub>2</sub> nanosheet composite piezoelectric films for energy harvesting. *Nano Energy*, **80**, 105541 (2021).  
<https://doi.org/10.1016/j.nanoen.2020.105541>
- [93] Khatua D. K., Raj N. P. M. J., Khandelwal G., Rao A. N., Kim S-J.: Tailoring mechanical energy harvesting performance of piezoelectric nanogenerator via intrinsic electrical conductivity of ferroelectrics. *Materials Today Energy*, **20**, 100679 (2021).  
<https://doi.org/10.1016/j.mtener.2021.100679>
- [94] Karan S. K., Maiti S., Kwon O., Paria S., Maitra A., Si S. K., Kim Y., Kim J. K., Khatua B. B.: Nature driven spider silk as high energy conversion efficient bio-piezoelectric nanogenerator. *Nano Energy*, **49**, 655–666 (2018).  
<https://doi.org/10.1016/j.nanoen.2018.05.014>
- [95] Zhang Y., Yang Y., Gu Y., Yan X., Liao Q., Li P., Zhang Z., Wang Z.: Performance and service behavior in 1-D nanostructured energy conversion devices. *Nano Energy*, **14**, 30–48 (2015).  
<https://doi.org/10.1016/j.nanoen.2014.12.039>
- [96] Beyaz M. İ., Tat F., Özkaya K. Y., Özbek R.: Hybrid magnetic-piezoelectric energy harvester for power generation around waistline during gait. *Journal of Electrical Engineering and Technology*, **15**, 227–233 (2020).  
<https://doi.org/10.1007/s42835-019-00309-4>